Dependence of projectile fragmentation on target *N/Z*

R. Laforest, E. Ramakrishnan, D. J. Rowland, A. Ruangma, E. M. Winchester, E. Martin, and S. J. Yennello
Cyclotron Institute, Texas A & M University, College Station, Texas 77843-3366
(Received 6 November 1998)

Peripheral reactions of ^{28}Si with ^{112}Sn and ^{124}Sn at 30, 40, and 50 MeV/nucleon were used to elucidate the effect of the neutron content of the target on the process of projectile fragmentation. It is demonstrated that the fragments that result from these projectile fragmentation reactions can be divided into those which are the result of statistical emission of the quasiprojectile and those that are part of a direct component. The statistical part is independent of the target whereas the isotopic composition of fragments from the direct component is dependent on the neutron content of the target. [S0556-2813(99)00305-2]

PACS number(s): 25.70.Mn, 25.70.Pq, 24.10.−i

I. INTRODUCTION

Projectile fragmentation has long been used to study the decay of excited nuclear systems [1–4]. It has traditionally been thought to be a two-step process consisting of excitation through a quasielastic collision followed by the breakup of the projectile [5–7]. In that scenario one could study the breakup of a hot nuclear system independent of the formation of the system. In fact much work has been done via projectile fragmentation to study whether the decay of excited nuclear matter is simultaneous or sequential [2,3]. Recently, it was shown that projectile breakup can occur in close proximity with the target and that particles are emitted in a mixture of statistical decay (either sequential or prompt) and by direct emission [1].

In the two-step model the target nucleus has no or limited effect on the fate of the decaying excited projectile. However, since projectile breakup occurs in peripheral collisions with the target and the excitation energy is determined by friction and nucleon exchange between the target and the projectile, the use of two targets with different neutron content could help us to discriminate between what was emitted by the breakup of the projectile and what was directly emitted at the time of contact. Moreover, a neutron-rich nucleus will have more neutrons at its surface, thus showing a neutron skin. This neutron skin results from the different proton and neutron density distributions at the surface of a heavy nucleus and has been predicted by theoretical calculations that include a proper asymmetry potential [8–10]. The differences caused by differing neutron content of the target may be best observed by looking at isotopically resolved fragments.

Isotopic indentification of emitted fragments has been used by several groups to study the dynamics of intermediate mass fragment (IMF) and light charged particle (LCP) emission [11–17]. These studies were done for midperipheral and central collisions. Recent microscopic transport calculations also revealed possible experimental signatures of isospin dependence within nuclear collisions [18–22]. The goal of this paper is to use the available isospin information to study the dynamics of fragment production and light charged particle emission in collisions where the dynamics was traditionally believed to have no effect.

II. EXPERIMENTAL SETUP

This experiment was done with a beam of ^{28}Si impinging on ~ 1 mg/cm^2 of ^{112,124}Sn self-supporting targets. The beam was delivered at 30, 40, and 50 MeV/nucleon by the K500 superconducting cyclotron at the Cyclotron Institute of Texas A & M University. Only the 30 and 50 MeV/nucleon data will be presented in this paper. The detector setup for this experiment is schematically depicted in Fig. 1. It is composed of an arrangement of 68 silicon-CsI(Tl) telescopes covering polar angles from 1.64° to 33.6° in the laboratory. Each element is composed of a 300-μm silicon detector followed by a 3-cm CsI(Tl) crystal. The detectors are arranged in five concentric rings. The geometrical efficiency is more than 90% for each ring. A more detailed description of the detectors and electronics can be found in Ref. [23] . These detectors allow for isotopic identification of light charged particles and intermediate-mass fragments up to a charge of $Z=5$. The energy thresholds are determined by the energy needed to punch through the 300-μm silicon detector. These thresholds are listed in Table I. These energy thresholds have little effect on the acceptance of particles from the fragmenting projectile, especially at 50 MeV/nucleon, due to the boost from the beam energy. However, these detector thresholds discriminate against low-energy particles originating from the target. This target fragment discrimination is consistent with our moving source fits to the data and GEMINI simulations.

Energy calibration of the silicon detectors was achieved with the use of a ^{228}Th α source providing six calibration points from 5.42 to 8.78 MeV. The CsI(Tl) detectors were calibrated from the measured energy loss in the silicon detector of a given particle of a certain mass and charge and from its total kinetic energy calculated with SRIM-96 [24]. This procedure [25] was used to determine the gain factor (a_0) which was common for all isotopes. The following equation [26] was used to relate the light output L of the CsI(Tl) crystal to the energy E of the particle:

$$L=\frac{a_0}{2}\int_0^E \frac{a_2(dE'/dx)(1+R)^2dE'}{2+a_2(dE'/dx)(1+R)}, \tag{1}$$

where

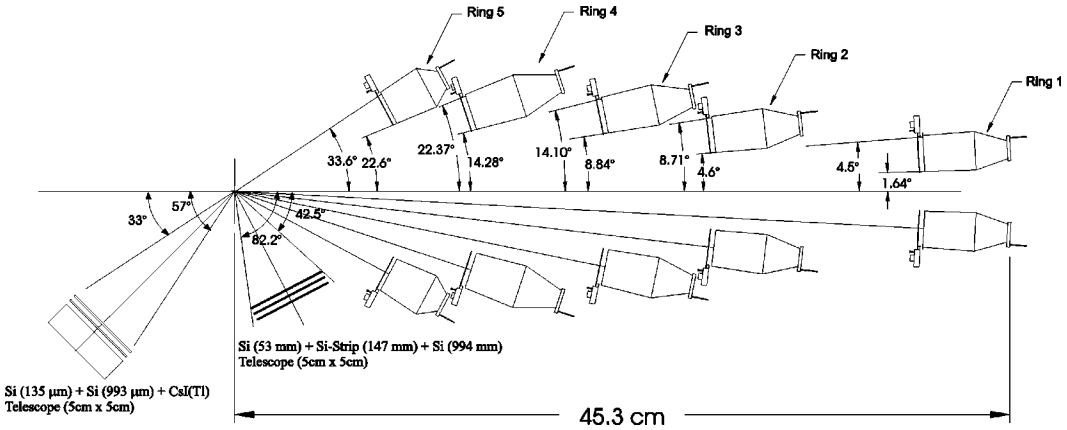

FIG. 1. Schematic side view of the experimental setup. The five Si-CsI(Tl) detector rings composing FAUST are shown. The two silicon telescopes and their angular coverage are also shown.

$$R=\frac{\ln(T_0/I_0)}{\ln[(a/I_0)(E/A)]}. \tag{2}$$

The parameters a, a_2, I_0, and T_0 are constants. dE/dx is the differential energy loss in CsI(Tl) calculated with SRIM-96, a is $4m_e/931.5$ MeV, and I_0 was set to 0.488 keV, the ionization potential of the scintillator. The other two parameters of this equation, a_2 and T_0, represent the light quenching in the CsI(Tl) due to the space-charge effect and the electron kinetic energy cutoff parameter [25]. These should be the same for all detectors and should depend on the intrinsic scintillation properties and light collection of the detector. It was checked that these two parameters were the same for all CsI(Tl) detectors. The values of a_2 and T_0 are 2.06 and 0.5 keV for $Z=1$, 2.6 and 9 keV for $Z=2$, and 2.87 and 2.31 keV for lithium and heavier elements. The parameters a_2 and T_0 were determined in a separate experiment where cocktail beams were produced from the fragmentation of ^{19}F at 35 MeV/nucleon on a 57 mg/cm^2 ^{12}C target. Fragments of specific momentum and charge were selected by the magnetic rigidity of the MARS beam line [27,28]. The energy of a particle for a given analog-to-digital converter (ADC) channel was obtained from an energy look-up table. In addition, the punchthrough points of hydrogen isotopes in CsI(Tl) crystals were also used. The overall procedure gives an energy resolution of typically 3%.

TABLE I. Energy thresholds for each particle type in the FAUST detector.

Particle	Threshold	Particle	Threshold (MeV)
^{1}H	6.1	^{10}B	100.7
^{2}H	8.2	^{11}B	104.4
^{3}H	9.6	C	133.1
^{3}He	21.8	N	168.8
^{4}He	24.6	O	206.3
^{6}LI	46.1	F	252.2
^{7}Li	49.2	Ne	289.4
^{7}Be	67.5	Na	339.5
^{9}Be	74.7	Mg	377
^{10}Be	77.9	Al	430
		Si	475

Additional silicon telescopes complemented the forward array in the setup. A telescope consisting of a 53-μm silicon detector, 147-μm silicon detector (16 strips), and a 994-μm silicon detector was placed at 40° in the laboratory. The 53-μm and 994-μm silicon detectors had an active area of 5 cm$\times$5 cm and were divided in four quadrants. This telescope covered the polar angle from 42.5° to 82.2°. Another silicon telescope was placed at 135° in the laboratory, covering polar angles from 123° to 147°. It was composed of two 5 cm$\times$5 cm active area silicon detectors of thickness 135-μm and 993-μm, respectively. A 2-cm-thick CsI(Tl) readout via a photodiode was placed behind both silicon pairs. The second telescope was used to detect light charged particles emitted by the target.

Figure 2 shows the pseudomomentum (sum of the charge multiplied by the parallel velocity) of all measured particles plotted as a function of total charge (sum of the charge) for

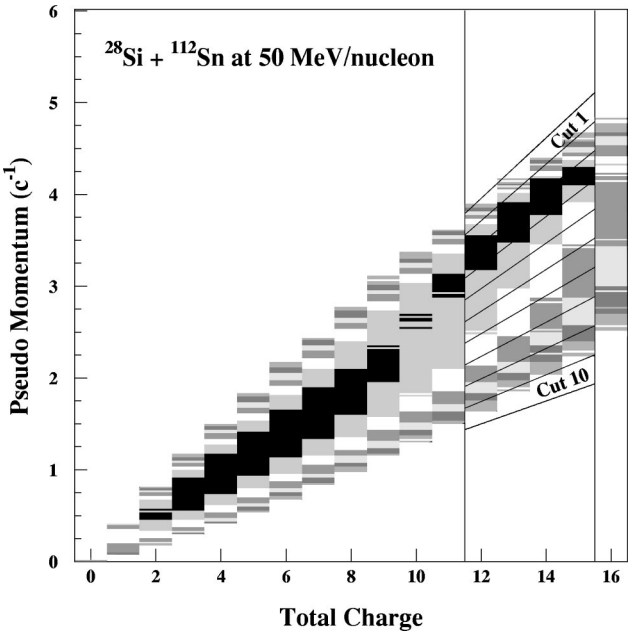

FIG. 2. Pseudomomentum plotted as a function of the total charge. The selection of quasiprojectile breakup events and the dissipation cuts are shown by the straight lines and are described in the text.

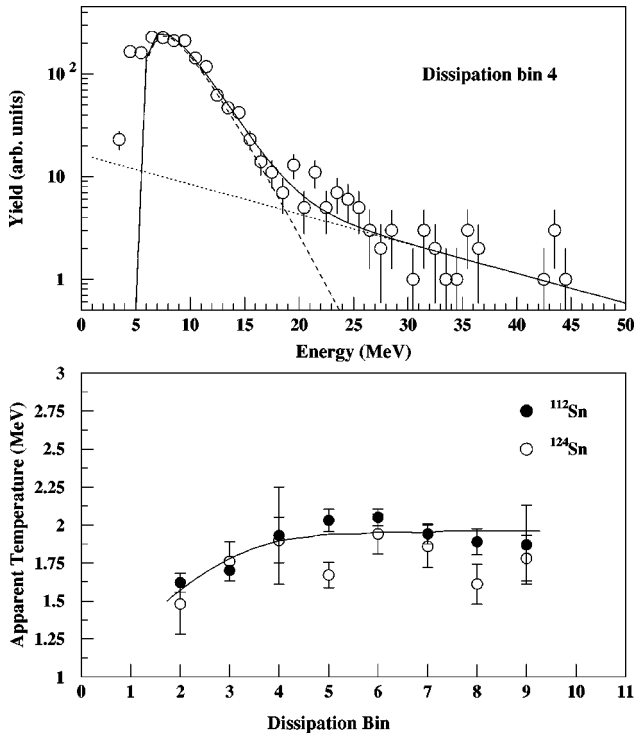

FIG. 3. Apparent temperature of target as measured from the kinetic energy spectra of protons. The top panel shows the kinetic energy spectra in the silicon telescope at backward angles. Lines show the result of a Maxwellian (dashed line) and exponential (dotted line) functions. The solid line represents the sum of these two distributions. The bottom panel shows the evolution of the apparent temperature as a function of dissipation for both targets. The solid line in the bottom panel is to guide the eye.

each event. The well-detected quasiprojectile breakup events can be easily identified in the upper right. The analysis performed for this paper deals only with events with a total detected charge of at least 12 and no more than 15, thus keeping only the quasiprojectile breakup events. The forward momentum was used as a control variable for the violence of the collisions. Since some of the fragments and LCPs emitted from the statistical decay of the target could not be detected due to the detector geometry and energy threshold, the amount of forward momentum was less for more violent collisions. Ten cuts in forward momentum were made and are labeled from 1 to 10. These cuts are shown in Fig. 2 by the diagonal lines. The lines are diagonal since as more particles are detected the pseudomomentum will be larger. Cut No. 1 corresponds to the least violent collisions and No. 10 to the most violent. Although it is reasonable to believe that more violent collisions imply a smaller impact parameter, no attempts were made to relate them. Each cut corresponds to a dissipation of approximately 500 GeV/c. One could have used the mass of the particle instead of the charge but this could lead to self-correlation in the ratios of yield that will be presented later in this paper.

The telescope at backward angles was used to detect particles emitted by the target. A measure of the temperature from Maxwellian fits of the proton energy spectra was extracted for the two targets at 50 MeV/nucleon. An exponential function had to be added for higher energies in order to achieve reasonable fits. This exponential corresponds to pre-

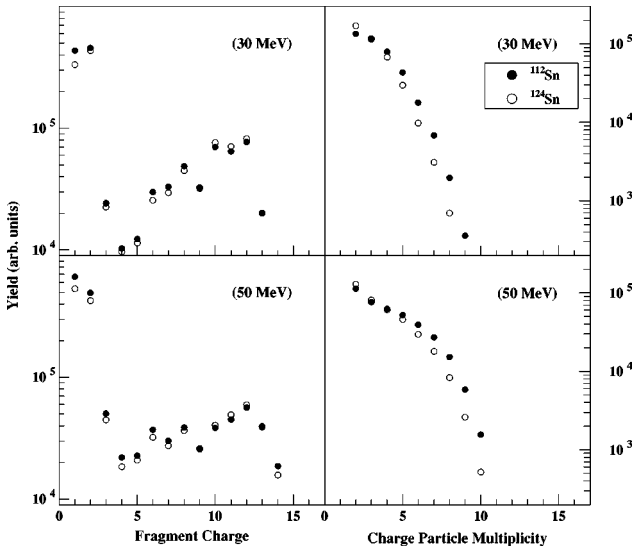

FIG. 4. Charged particle distribution and multiplicity at 30 and 50 MeV/nucleon. Open circles correspond to data obtained with ^{124}Sn target, and solid circles to ^{112}Sn target. The same notation will be used in the rest of the paper.

equilibrium emission at backward angles, an effect that has been previously reported [29]. Figure 3 shows an example of one fit and the relation between the apparent temperature and dissipation. It shows a slow increase in the temperature as a function of violence followed by saturation. This rise and saturation of the target temperature will be shown in another paper [30]. The apparent temperatures from the Maxwellian distributions have a value of approximately 2 MeV. The preequilibrium contribution observed for protons has a slope parameter of around 15 MeV. Both targets have approximately the same temperature. As the projectile loses more of its kinetic energy in colliding with the target, the overlap zone becomes more excited, but the target stays approximately at the same temperature. Only at small dissipation, or for more peripheral collisions, do we observe an increase of target temperature, the latter being the consequence of a binary collision.

Figure 4 shows the charge distribution and charged particle multiplicity distribution obtained for particles detected in the forward array for the quasiprojectile breakup events. One can see that the events are mostly composed of a projectilelike fragment (PLF) accompanied by light charged particles. The distributions were normalized for the same number of events for the two targets at a given beam energy. The ^{112}Sn target produces slightly more $Z=1$ and $Z=2$ particles which results in slightly larger multiplicities. The 50 MeV/nucleon data reveal a smaller PLF and larger multiplicities due to the increase of excitation in the quasiprojectile. The larger proton yield with the ^{112}Sn target can be also interpreted by more preequilibrium or direct emission due to the peripheral nature of the collision. In a grazing collision with a more neutron-rich target like ^{124}Sn, this preequilibrium emission could appear in the neutron multiplicities which were not measured in this experiment. This would be consistent with a neutron skin at the surface of the target.

III. ISOTOPIC RATIOS

We know from previous experiments that statistical decay (sequential or prompt) is known to be important for projec-

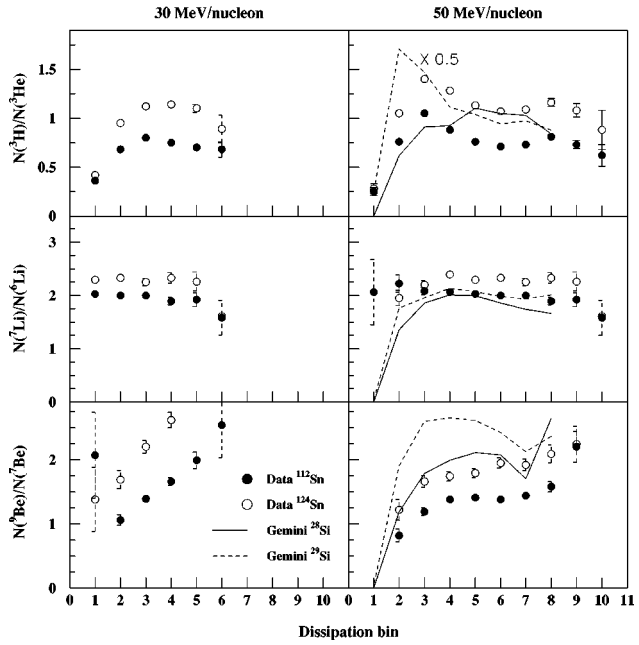

FIG. 5. Ratio of yield of different isotopes at 30 (left) and 50 (right) MeV/nucleon. From top to bottom, this figure shows the ratio of yield of ^{3}H to ^{3}He, ^{7}Li to ^{6}Li, and ^{9}Be to ^{7}Be. At 50 MeV/nucleon, the solid and dashed lines correspond to GEMINI calculation of the decay of ^{28}Si and ^{29}Si, respectively. Open circles correspond to data obtained with the ^{124}Sn target, and solid circles to the ^{112}Sn target.

tile fragmentation events. However, as was pointed out in Ref. [1], the short decay times and fragment correlation show a mixture of statistical and direct emission. The use of two Sn targets allows us to determine what was the contribution from the target in terms of nucleon transfer to the projectile, or in the excitation of the latter. In an excitation followed by breakup that is purely independent of the target, no difference whatsoever should be observed.

Figure 5 shows the ratios of isotope yields plotted for the different degrees of violence of the collisions shown in Fig. 2. The top panels show the ratios of the yield of ^{3}H to ^{3}He for the two targets at 30 and 50 MeV/nucleon. More ^{3}He than ^{3}H are observed at all dissipation for ^{112}Sn target compared to the ^{124}Sn target. At 50 MeV/nucleon a bump is seen at small dissipation. This could be due to a small probability of neutron pickup by the quasiprojectile at small dissipation as indicated by the following simulation.

GEMINI calculations for the decay of the ^{28}Si excited projectile were performed in order to tell us what would result if the yield of fragments and LCPs were solely due to the statistical decay of the projectile. The input distributions for GEMINI, excitation energy, and quasiprojectile velocity distribution were obtained from the experimentally reconstructed velocity distribution and excitation energy distribution assuming that all detected particles come from the decay of the projectile. This is not exact since some particles are emitted directly. Nevertheless, the simulation should give a good estimate of the statistical emission.

In the simulation, we first sample the reconstructed quasiprojectile velocity by Monte Carlo simulations. This velocity is used to boost the velocities of particles calculated in the center of mass of the emitter to the laboratory reference frame. This allows the results of the simulation to be treated exactly as if they were experimental data. The simulation results were filtered through a detailed software replica of the detector setup. The quasiprojectile excitation energy is obtained from the experimental relation between quasiprojectile velocity and excitation energy. In this way, a selection in violence by a cut on the forward pseudomomentum results in selecting events with a higher excitation energy. It was verified that cuts on the excitation energy of the projectile yield the same ratios.

Also, in order to simulate the contribution from the pickup of one neutron by the projectile, the decay of ^{29}Si was simulated with GEMINI using the same quasiprojectile and excitation energy distribution. Those simulations are represented by the solid and dashed lines in Fig. 5. They were performed only at 50 MeV/nucleon. For the ratio of ^{3}H to ^{3}He yields, the ^{29}Si simulation was divided by 2 in order to plot it on the same graph. This plot indicates that if there is some neutron pickup by the quasiprojectile, it represents only a small contribution to the ratios at all dissipation. Mostly neutron pickup will produce larger ratios at small dissipation and would account for the small bump observed for both targets. The lack of a bump in the 30 MeV data could be due to the relative closeness of the kinetic energy of the projectile at 50 MeV/nucleon and the Fermi energy of a neutron in the target. This small relative energy could result in a higher neutron capture cross section.

The ratio of Li isotopes (^{7}Li over ^{6}Li) again shows a larger yield of the neutron-rich Li from the ^{124}Sn target to the ^{112}Sn target but to a smaller extent. The ratios predicted by GEMINI are very comparable and are identical for ^{28}Si and ^{29}Si, showing that if there is any neutron pickup, it will not affect the ratio of Li isotopes. The ratio of Be isotopes (^{9}Be/^{7}Be) again shows larger yields of neutron-rich Be for all dissipation values. Ratios predicted by GEMINI are also close to the experimental values but are not exact.

The fact that there is a difference between the two targets for all dissipation bins indicates that fragments are not emitted only by the decay of the projectile, but that dynamical processes like neck breakup also contribute to fragment production.

At 30 MeV/nucleon, we still produce more neutron-rich fragments from the more neutron-rich target but the independence of the ratios over the range of dissipation values is no longer observed. The Be isotope ratios show a big increase for larger dissipation. This shows that neutron-rich fragments are produced with the neutron-rich target for a sufficiently large overlap of the projectile with the target. This suggests that as the projectile spends more time in the neutron-rich target skin due to its slower relative velocity, isospin equilibration will favor a neck with more neutrons.

The ratios in Fig. 5 were plotted as a function of the total dissipation. In Fig. 6 we plot different ratios of isotopes as a function of the velocity of the particles at 30 MeV/nucleon and at 50 MeV/nucleon. The two panels show the isobaric ratios of ^{3}H/^{3}He, and ^{7}Be/^{7}Li. Slower particles are more likely to be emitted by a slow-moving source. The beam energy dependence of these ratios may tell us something about the degree of isospin equilibrium achieved for different beam velocities. The data shown here are above the threshold velocity for the ^{3}He. At 30 MeV/nucleon, the

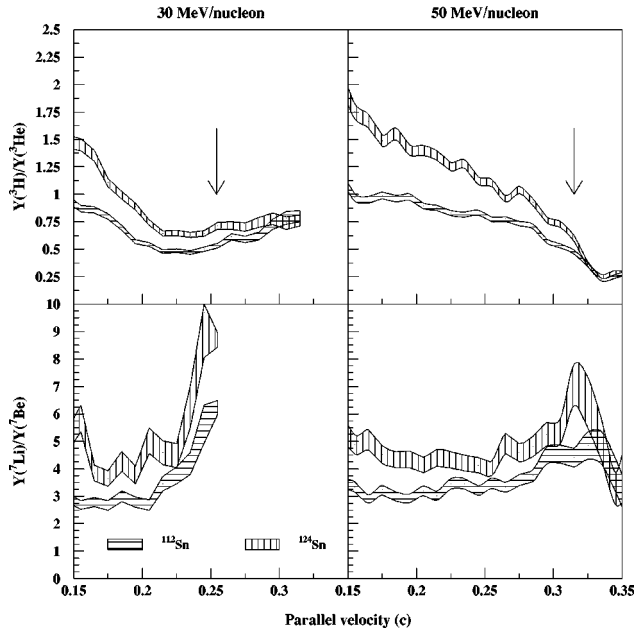

FIG. 6. Ratio of yields of ^{3}H to ^{3}He are presented in the top panels at 30 (left) and 50 (right) MeV/nucleon plotted as a function of particle velocity. The bottom panels show the ratios of ^{7}Be to ^{7}Li at the two energies. Horizontal and vertical hatched zones correspond to data from the two targets ^{112}Sn and ^{124}Sn, respectively. Errors are indicated by the width of the hatched area; arrows indicate the beam velocity.

^{3}H/^{3}He ratio decreases from small to large velocities and becomes constant close to beam velocity and then remains constant above beam velocity. At 50 MeV/nucleon, the ratio of ^{3}H to ^{3}He exhibits a continuous decrease for higher particle velocity. For heavier isotopes, the ratios are essentially the same at all velocities with the exception that close to the beam velocity a sharp bump is observed. The bump around the beam velocity may be due to a small contribution from neutron pickup. Ratios are always larger for the ^{124}Sn target.

These observations are consistent with the observation of a neutron-rich neck reported before [11,12]. The fact that the ratios are equal for both targets above projectile velocity suggests a strong statistical contribution from quasiprojectile breakup close to beam velocity only. At lower velocities, breakup of the neck, which is more neutron rich for the ^{124}Sn target, is responsible for the increase in the ratio.

The angular distributions of the ratios of yields at 50 MeV/nucleon are shown in Fig. 7. In this figure, we can observe larger ratios of ^{3}H/^{3}He yield at larger angles. This also shows that the directly emitted particles are emitted at larger laboratory angles than those emitted by the in-flight decay of the quasiprojectile. This implies that the neutron-rich LCPs come from a more neutron-rich neck region. The same behavior is observed for the two energies. For heavier isotopes, the ratios are essentially flat.

IV. LIGHT CHARGED PARTICLE VELOCITY SPECTRA

The in-flight decay of the projectile will produce velocity spectra of light charged particles that have a Gaussian shape, centered at the quasiprojectile velocity. Figure 8 shows parallel velocity spectra for three breakup channels Na+3^{1}H,

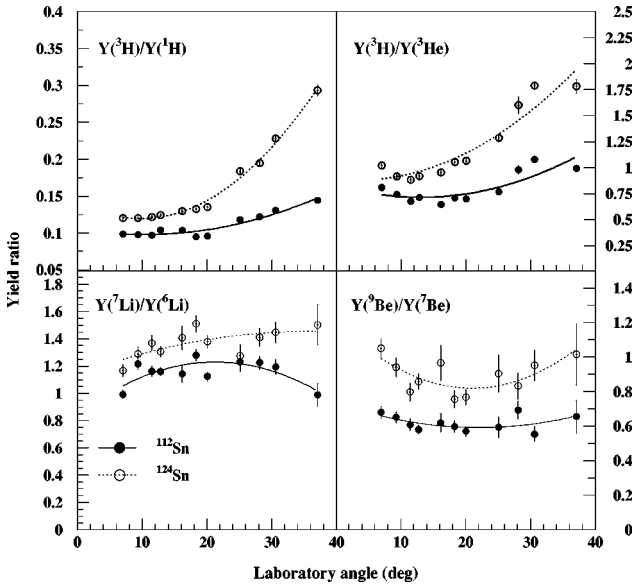

FIG. 7. The angular distributions of ratios of yields of ^{3}H to ^{1}H, ^{3}H to ^{3}He, ^{7}Li to ^{6}Li, and ^{9}Be to ^{7}Be are presented for the 50 MeV/nucleon data. Open circles correspond to data obtained with the ^{124}Sn target, and solid circle to the ^{112}Sn target. Lines are drawn to guide the eye.

Ne+2^{4}He, and Na+^{4}He+1H at 50 MeV/nucleon. These three channels are typical and define three categories: PLF + hydrogen isotopes, α-like, and mixed channels. α-like channels correspond to channels containing only α particles and α-clustered nuclei. Mixed channels correspond to breakup channels containing α particles and hydrogen isotopes. These velocity distributions were normalized to the same number of events for each target. The ^{112}Sn target results in a much larger yield for the channels containing a PLF and protons only. This is probably due to the contribution of

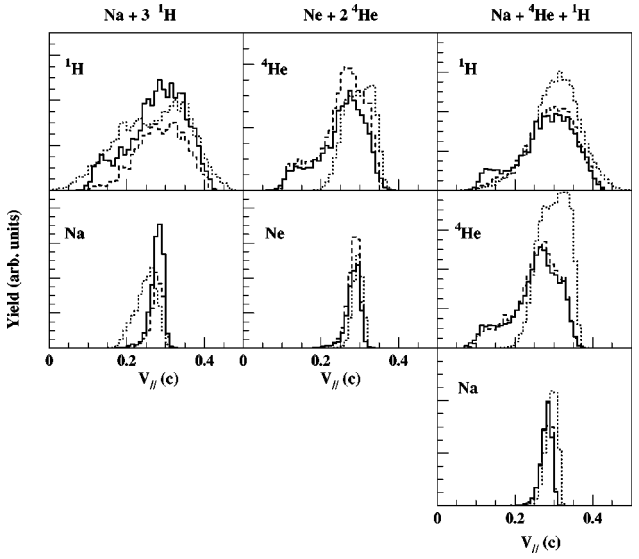

FIG. 8. Parallel velocity spectra of the particles composing three typical fragmentation channels. Solid, dashed, and dotted lines represent data from the ^{112}Sn target, ^{124}Sn target, and the result of a GEMINI calculation, respectively, for the decay of ^{28}Si at 50 MeV/nucleon.

directly emitted protons. We can observe here that the spectra are very similar for both targets except for the low-velocity tail which is more important for the neutron-poor target. The ^{124}Sn target yields a slightly larger amount of α-like channels and similar amounts of mixed channels when compared to the ^{112}Sn target.

This figure also shows that GEMINI fits the velocity distribution of the projectilelike fragment well. The calculation shows that while the PLF velocity spectra are fitted, only the high-velocity part of the light charged particles spectra can be reproduced for all but protons. The lower-velocity part of the spectra for the α particles is seen to be the same for both targets, whereas the low-energy tails of the protons are substantially different for the two targets.

An estimate of the light charged particles emitted by stastical decay of the excited quasiprojectile can be extracted for the total yield in the following manner. Particles emitted in the forward direction relative to the projectilelike fragment are considered to be produced by the in-flight decay of the quasiprojectile. This forward contribution as well as its reflection around the projectilelike fragment velocity is then subtracted from the total yield to extract the yield of the direct component. Figure 9 shows the parallel velocity distribution of LCPs where the forward contribution (plus its reflection) is removed (see inset). These spectra were created in the reference frame of the PLF for events containing a projectilelike fragment of charge 6 or heavier. In order to take into account the differential target Coulomb repulsion that results in velocity shifts [1], the reflection was performed around a small offset relative to the PLF. The offsets were determined by the centroid of a Gaussian distribution fitted on the forward side of the distribution. These offsets were set to zero for deuterons and alpha particles since those have $N/Z=1$. The offset was set to a small positive value for protons and ^{3}He, and to a small negative number for ^{3}H. The necessity of considering different velocity shifts in the reacceleration in the target Coulomb field is due to the short decay time of the quasiprojectile (QP). The decay was estimated to occur within 15 fm from the target in a similar reaction [1]. The same method and offsets were applied for both targets. The ratios of detected particles, normalized to the same number of events for both targets, obtained by this method are summarized in Table II.

All ratios are close to 1 for the quasiprojectile decay component, meaning that the excited projectiles produced are fairly identical for both targets. However, the direct emission component differs substantially. A lot more protons and ^{3}He are directly emitted by a grazing collision with a neutron poor target than can be expected. Also, the number of ^{3}H directly emitted is significantly less for the ^{112}Sn target while the number of deuterons and alphas remains approximately the same. The statistical errors in those ratios are at most 5% (typically 1%). An evaluation of the systematic error was performed by changing the velocity offsets by a small amount and resulted in fluctuations of at most 20% in the evaluation of the ratios of the direct component only. The systematic errors for the quasiprojectile decay component evaluated by this method are very small.

V. CONCLUSIONS

This paper shows that projectile fragmentation depends on the N/Z of the target because fragment and light charge particle emission appears as a mixture of directly emitted light charged particles, neck rupture for the fragments, and statistical decay of the excited quasiprojectile.

The determination of the violence of the collisions with forward momentum showed that the target temperature satu-

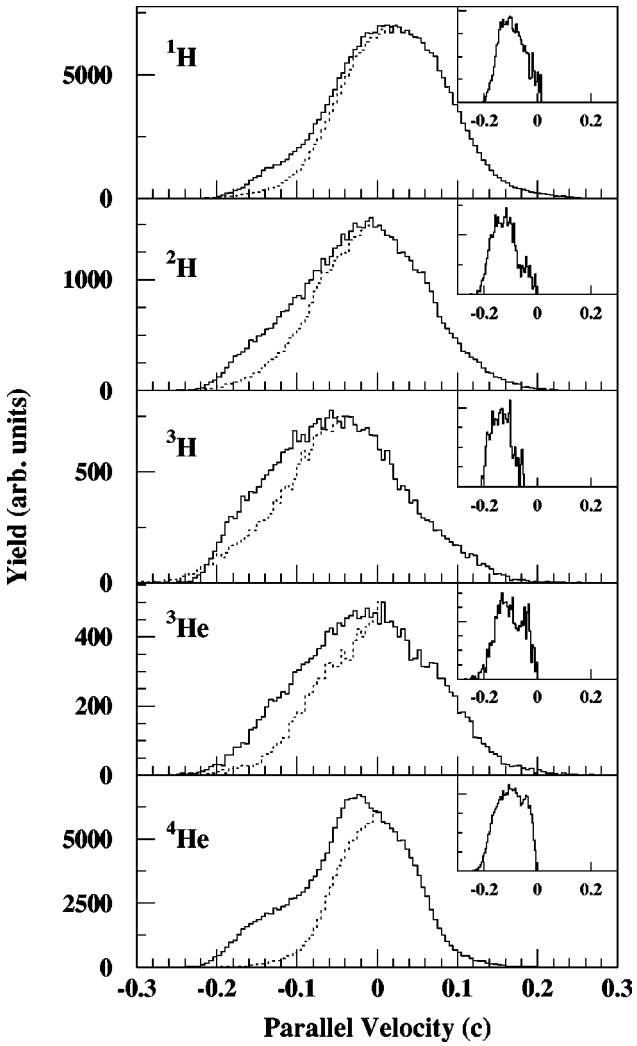

FIG. 9. Parallel velocity spectra of light charged particles in the PLF reference frame from the reaction of ^{28}Si+^{112}Sn at 50 MeV/nucleon. The solid line represents the total velocity spectrum. The dotted line represents the projectile decay component. The inset shows the subtraction of the projectile decay component from the total spectrum, yielding the direct component.

TABLE II. Yields of light charged particles from reconstructed events of ^{28}Si+^{112}Sn at 50 MeV/nucleon divided by the yields from ^{28}Si+^{124}Sn. The ratios were normalized for the same number of events for both targets. All LCPs were measured in the range of 1.64°–33.6° in the laboratory.

Particle	Overall	QP decay	Direct emission
^{1}H	1.36	1.24	2.58
^{2}H	1.15	1.11	1.40
^{3}H	0.96	1.01	0.53
^{3}He	1.32	1.23	1.74
^{4}He	1.12	1.10	1.18

rates at approximately 2 MeV. In addition, for the more violent collisions, we observed larger multiplicities emitted from the neck. This is in agreement with a larger geometrical overlap between the projectile and the target.

The multiplicity distribution of charged particles is larger for the reaction on the ^{112}Sn target. This is related to the shift in the charge distribution which has more smaller particles and fewer heavy particles with the ^{112}Sn target relative to the ^{124}Sn target. More neutron-rich light particles arise from the neck region as seen in the velocity distribution and angular distribution of the isotope ratios. This effect is enhanced for the more neutron-rich target. When the contribution due to statistical emission from the quasiprojectile is factored out the direct component reflects the relative neutron content of the target.

ACKNOWLEDGMENTS

The authors wish to thank the Cyclotron Institute staff for the excellent beam quality. This work was supported in part by the NSF through Grant No. PHY-9457376, the Robert A. Welch Foundation through Grant No. A-1266, and the Department of Energy through Grant No. DE-FG03-93ER40773.

[1] R. J. Charity, L. G. Sobotka, N. J. Robertson, D. G. Sarantities, J. Dinius, C. K. Gelbke, T. Glasmacher, D. O. Handzy, W. C. Hsi, M. J. Huang, W. C. Lynch, C. P. Montoya, G. F. Peaslee, C. Schwarz, and M. B. Tsang, Phys. Rev. C **52**, 3126 (1995).

[2] R. Laforest, D. Dore, J. Pouliot, R. Roy, C. St-Pierre, G. Auger, P. Bricault, S. Groult, E. Plagnol, and D. Horn, Nucl. Phys. **A568**, 350 (1994).

[3] B. Harmon, J. Pouliot, J. A. Lopez, J. Suro, R. Knop, Y. Chan, D. E. Digregorio, and R. G. Stockstead, Phys. Lett. B **235**, 234 (1990).

[4] J. Pouliot, Y. Chan, D. E. DiGregorio, B. A. Harmon, R. Knop, C. Moisan, R. Roy, and R. G. Stockstead, Phys. Rev. C **43**, 735 (1991).

[5] L. Beaulieu, R. Laforest, J. Pouliot, R. Roy, C. St-Pierre, G. C. Ball, E. Hagberg, D. Horn, and R. B. Walker, Nucl. Phys. **A580**, 81 (1994).

[6] A. Badal'a, R. Barbera, A. Palmeri, G. S. Pappalardo, F. Riggi, G. Bizard, D. Durand, and J. L. Laville, Phys. Rev. C **45**, 1730 (1992).

[7] R. Charity, J. Barreto, L. Sobotka, D. G. Sarantites, D. W. Stracener, A. Chbihi, H. G. Nicolis, R. Auble, C. Baktash, J. R. Beene, F. Bertrand, M. Halbert, D. C. Hensley, D. J. Horen, C. Ludemann, M. Thoennessen, and R. Varner, Phys. Rev. C **46**, 1951 (1992).

[8] L. G. Sobotka, J. F. Dempsey, R. J. Charity, P. Danielewicz, Phys. Rev. C **55**, 2109 (1997).

[9] L. G. Sobotka, Phys. Rev. C **50**, R1272 (1994).

[10] Z. Z. Ren, W. Mittig, B. Q. Chen, and Z. Y. Ma, Phys. Rev. C **52**, 20 (1995).

[11] J. F. Dempsey, R. J. Charity, L. G. Sobotka, G. J. Kunde, S. Gaff, C. K. Gelbke, T. Glasmacher, M. J. Huang, R. C. Lemmon, W. G. Lynch, L. Manduci, L. Martin, M. B. Tsang, D. K. Agnihotri, B. Djerroud, W. U. Schröder, W. Skulski, J. Toke, and W. A. Friedman, Phys. Rev. C **54**, 1710 (1996).

[12] E. Ramakrishnan, H. Johnson, F. Gimeno-Nogues, D. J. Rowland, R. Laforest, Y.-W. Lui, S. Ferro, S. Vasal, and S. J. Yennello, Phys. Rev. C **57**, 1803 (1998).

[13] S. J. Yennello, B. Young, J. Yee, J. A. Winger, J. S. Winfield, G. D. Westfall, A. Vander Molen, B. M. Sherrill, J. Shea, E. Norbeck, D. J. Morrissey, T. Li, E. Gualtieri, D. Craig, W. Benenson, and D. Bazin, Phys. Lett. B **321**, 15 (1994).

[14] S. J. Yennello, E. Ramakrishnan, H. Johnson, G. Gimeno-Nogues, D. J. Rowland, R. Laforest, Y.-W. Lui and S. Ferro, in Proceedings of the VI International Summer School on Heavy-Ion Physics, Dubna, Russia, 1997.

[15] S. J. Yennello, R. Laforest, E. Martin, E. Ramakrishnan, D. J. Rowland, A. Ruangma, and E. Winchester, in Proceedings of the XXXVI International Winter Physics Meeting, Bormio, Italy, 1998.

[16] H. Johnston, T. White, J. Winger, D. Rowland, B. Hurst, F. Gimeno-Nogues, D. O'Kelly, and S. J. Yennello, Phys. Lett. B **371**, 186 (1996).

[17] H. Johnston *et al.*, Phys. Rev. C **56**, 1972 (1997).

[18] M. Colonna, M. Di Toro, G. Fabbri, and S. Maccarone, Phys. Rev. C **57**, 1410 (1998).

[19] Bao-An Li, C. M. Ko, and Z. Ren, Phys. Rev. Lett. **78**, 1644 (1997).

[20] Bao-An Li, Z. Ren, C. M. Ko, and S. J. Yennello, Phys. Rev. Lett. **76**, 4492 (1996).

[21] Bao-An Li and S. J. Yennello, Phys. Rev. C **52**, R1746 (1995).

[22] Bao-An Li and C. M. Ko, Phys. Rev. C **57**, 2065 (1998).

[23] F. Gimeno-Nogues, D. J. Rowland, E. Ramakrishnan, S. Ferro, S. Vasal, R. A. Gutierrez, R. Olsen, Y. W. Lui, R. Laforest, H. Johnson, and S. J. Yennello, Nucl. Instrum. Methods Phys. Res. A **399**, 94 (1997).

[24] J. P. Biersack and J. F. Ziegler, computer code SRIM-96 (stopping and range of ion in matter), 1996.

[25] D. Fox, D. R. Bowman, G. C. Ball, A. Galindo-Uribarri, E. Hagberg, D. Horn, L. Beaulieu, and Y. Larochelle, Nucl. Instrum. Methods Phys. Res. A **374**, 63 (1996).

[26] D. Fox (private communication).

[27] R. Tribble, R. H. Burch, and C. A. Gagliardi, Nucl. Instrum. Methods Phys. Res. A **285**, 441 (1989).

[28] R. Laforest, Progress in Reseach, TAMU, 1997.

[29] W. Skulski, M. Fatyga, K. Kwiatkowski, H. Karwowski, L. W. Woo, and V. E. Viola, Phys. Lett. B **218**, 7 (1989).

[30] Y. Larochelle, C. St-Pierre, L. Beaulieu, N. Colonna, L. Gingras, G. C. Ball, D. R. Bowman, M. Colonna, G. D'Erasmo, E. Fiore, D. Fox, A. Galindo-Uribarri, E. Hagberg, D. Horn, R. Laforest, A. Pantaleo, R. Roy, and G. Tabliente, Phys. Rev. C **59**, R656 (1999).